Clays Clay Miner., Vol. 70, No. 5:712–732, 2022
https://doi.org/10.1007/s42860-022-00212-6

ORIGINAL PAPER

Facies, Geochemistry, and Ceramic Properties of Corumbataí Formation, Upper Permian of Paraná Basin, and its Application in the Ceramic Industry, Brazil

Sergio Ricardo Christofoletti · Alessandro Batezelli · Maria Margarita Torres Moreno

Accepted: 3 November 2022 / Published online: 30 November 2022

Abstract The supply of Corumbataí Formation rocks, which occur widely in the State of São Paulo, Brazil, and are used by Santa Gertrudes Ceramic Cluster, is dwindling and prospecting for new deposits is essential. The current study aimed to map and characterize new reserves of ceramic raw materials which would guarantee mineral and economic sustainability of the important concentration of ceramic-processing capability in that area, and thereby contribute to improving and diversifying the range of products manufactured and to promoting a greater presence in the international market. To achieve the proposed objectives, 16 profiles were sampled and the samples were submitted to granulometric analysis by laser diffraction, and the major elements by inductively coupled plasma-mass spectrometry, and the mineralogical compositions of clay samples were determined by X-ray diffraction and ceramic properties. Six lithofacies were identified and grouped into two facies associations: a lower shoreface association comprising massive siltstone (Sm) and laminated siltstone (Sl); lithofacies, and an upper shoreface association comprising heterolithic sandstone (Sh), lenticular sandstone (Sle), intercalated sandstone/siltstone (Si), and altered siltstone (Sa) lithofacies. The lithofacies of the lower shoreface association were more clayey, flux with a significant presence of illite and microcline, and a more uniform granulometry distribution, which made its classification possible, technologically, as stoneware and semi stoneware. The main application of this material is in the production of coatings through the wet milling process. The lithofacies of the upper shoreface association was sandier, had a refractory presence with kaolinite and montmorillonite, and had a less uniform granulometric distribution; technologically, it can be characterized as porous and semi-porous. The main application of this material is in the production of coatings by the dry milling process. The results obtained by facies analysis combined with the geochemical and ceramic properties of the Corumbataí Formation rocks revealed both vertical and lateral variations of the lithofacies, which influence their properties, behavior, and application as ceramic raw materials.

Keywords Ceramic raw materials · Clay · Corumbataí Formation · Lithofacies

Associate Editor: Selahattin Kadir.

S. R. Christofoletti (✉)
IPA – Environmental Research Institute, Secretary of the Infrastructure and Environment/ FEENA, Rio Claro, SP, Brazil
e-mail: sergioricardoc@gmail.com

A. Batezelli
Geosciences Institute, Unicamp, Campinas, SP, Brazil

M. M. T. Moreno
Geosciences and Exact Sciences Institute, UNESP, Rio Claro, SP, Brazil

Introduction

Clays or clayey rocks have numerous applications and are important in various industrial and environmental sectors (Murray, 1999; Bergaya & Lagaly, 2006). In the ceramic industry, they play a key role in the production of complex products, as well as in processes used in the production of electronic components in advanced ceramics and in the production of blocks and bricks obtained from structural ceramics (Smoot, 1961). Several authors have studied clay deposits as a source of raw material for the ceramic-tile industry (Beltrán et al., 1996; Boix et al., 1994; Dondi, 1999; Dondi et al., 2014; Ferrari & Gualtieri, 2006; Fiori, 1996; Galos, 2011; Kadır et al., 2011; Külah et al., 2014; Manju et al., 2001; Zalba, 1979; Zanelli et al., 2008, 2015).

The Corumbataí Formation, a geological unit of the Paraná Basin of Permian age, contains one of the largest deposits of raw materials for the ceramic industry in Brazil (Christofoletti et al., 2009; Motta et al., 2004, 2005). It occurs widely in the State of São Paulo, and is used with great success in the Ceramic Cluster of Santa Gertrudes in the production of tiles, currently representing the largest ceramic center in the Americas, with an annual installed production of 812.29 million square meters per year of ceramic tile, having produced, in 2020, 538.32 million square meters, 87% being processed by dry grinding and 13% by wet (Aspacer, 2021).

Two types of mass -preparation processes are used in the manufacture of ceramic tile in Brazil: the dry process, more common, in which Ceramic Cluster of Santa Gertrudes leads the world. It uses the clayey rocks of the Corumbataí Formation as a unique raw material, where the mass is ground, moistened, and pressed, generating semi-porous products as the main product; the other process is the wet process, where the mass is composed of a combination of raw materials, where these are fractionated and granulated through a 'spray dryer' (atomizer), generating stoneware and porcelain as the main products.

Because of its economic importance, several studies have been carried out in the deposits near Santa Gertrudes Ceramic Cluster in order to understand the geological, geochemical, and technological characteristics. The facies concept was applied by Christofoletti et al. (2006), following initial description by Miall (1994), to the description and mapping of ceramic lithofacies in addition to technological, mineralogical, and chemical identification of the properties. Other studies focused on other discoveries (Azzi et al., 2016; Christofoletti et al., 2010, 2018; Del Roveri et al., 2016; Montibeller et al., 2020; Motta et al., 2010; Zanardo et al., 2016.). Preliminary results from one of those studies were presented by Christofoletti et al. (2015). Studies of the economic use of these deposits in the area are scarce; only Souza Campos et al. (2010) and Meneghel (2021) have otherwise studied these clays, seeking improvement and diversification of products in the Santa Gertrudes Ceramic Cluster.

Although the deposits of these rocks are large in the State of São Paulo, they show significant variations in their facies throughout the occurrence (Sousa, 1985); these variations are important in determining whether or not the materials can be used as raw materials for ceramics. In the region of the Santa Gertrudes Ceramic Cluster, the deposits have become increasingly scarce due to inefficient mining, urban expansion, increased environmental restrictions, and competition from other forms of land use, especially the expansion and strengthening of agricultural activity in sugar cane crops (Christofoletti & Moreno, 2011).

In order to guarantee the economic and environmental sustainability of the Santa Gertrudes Ceramic cluster, the present study sought to discover and evaluate new deposits in the Corumbataí Formation. The facies identification helped in the preliminary interpretation of the depositional and diagenetic environments of formation of those deposits.

Study Area and Geological Setting

The area that was studied is in the northeast of the state of São Paulo, around the cities of Porto Ferreira, Tambaú, and Santa Rosa de Viterbo (Fig. 1). Porto Ferreira is known as the capital of artistic ceramics. The raw materials for manufacturing those products come from other regions, however. Tambaú represents one of the state ceramic clusters that produce structural ceramics, where material from the upper layers of the Corumbataí Formation are used in the production of tiles and bricks, and in the composition of masse for various ceramic coating companies by the wet ceramic grinding process. Santa Rosa do

https://doi.org/10.1007/s42860-022-00212-6 Published online by Cambridge University Press

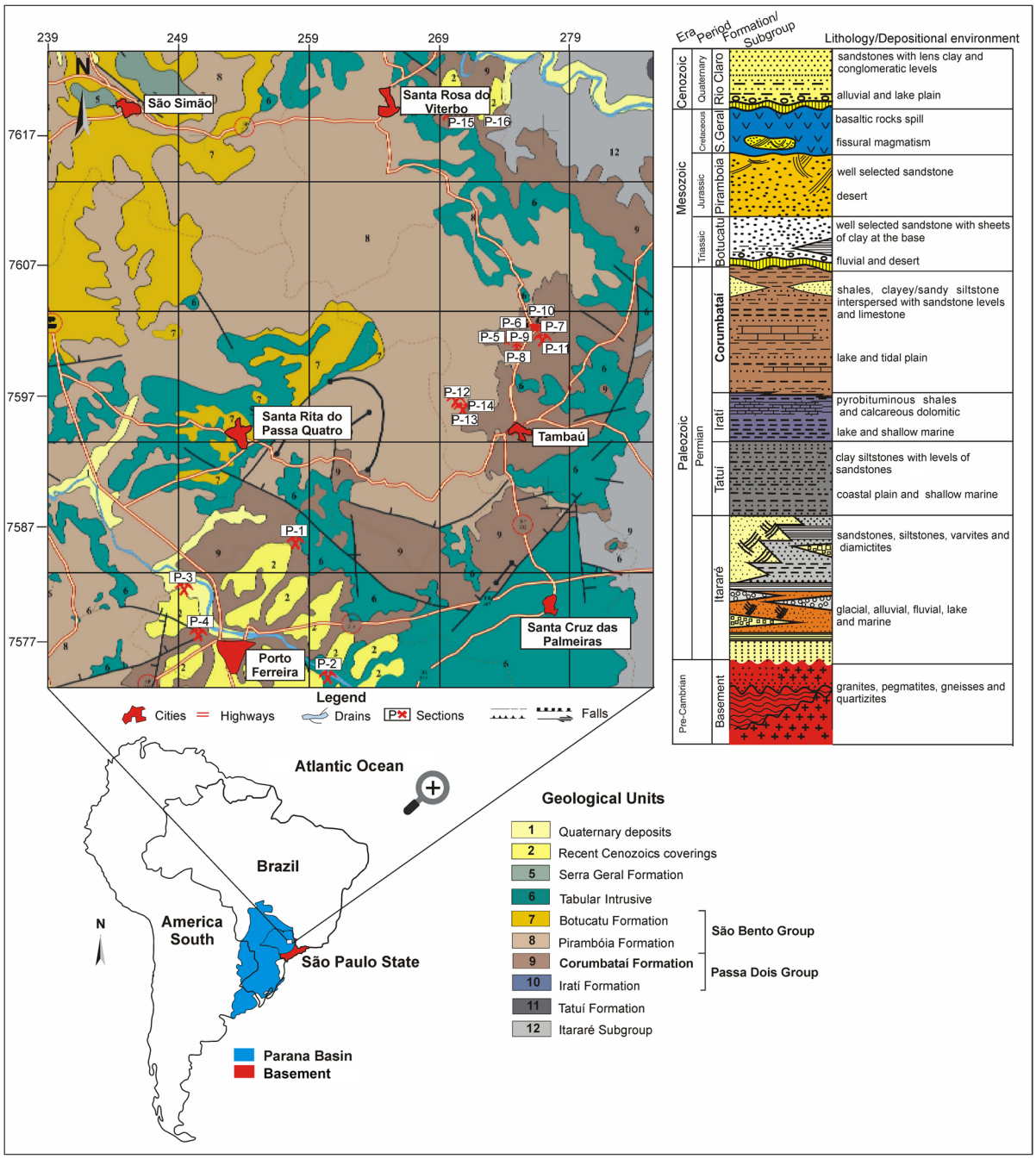

Fig. 1 Geological map of the study area. Below is the South American Continent, including Brazil and the Paraná Sedimentary Basins. A simplified stratigraphic column is given on the right (modified from Perinotto & Zaine, 2008)

Viterbo contains only one clay mine of the Corumbataí Formation, where the raw material is marketed to various ceramic industries to form a proportion of processed formulations via wet grinding.

Geologically, the area that has been studied is in the Paraná Basin, which is a geotectonic entity located in the southeast part of the South American plate, covering an area of 1,600,000 km^2. Most of

https://doi.org/10.1007/s42860-022-00212-6 Published online by Cambridge University Press

that area is in Brazilian territory (~1,000,000 km^2), distributed in the states of Rio Grande do Sul, Santa Catarina, Paraná, São Paulo, Mato Grosso do Sul, Mato Grosso, Minas Gerais, and Goiás (Milani, 1997). In the studied region, the following lithostratigraphic units occur from the bottom to the top, Itararé Subgroup, Passa Dois Group (Irati and Corumbataí Formations), São Bento Group (Pirambóia and Botucatu Formations), basic intrusive rocks of Serra Geral Formation, and culminating in Quaternary sediments and recent Cenozoic coverings (Fig. 1).

According Mezzalira (1964), the term Corumbataí was first described initially by the Geographical and Geological Survey of São Paulo in a 1916 report as "clay and bituminous schist with fossils." The Corumbataí Formation was referred to (Landim, 1970) as "the essentially clayey sedimentary rocks of reddish or purplish color with interleaves of fine sandstone lenses in the Corumbataí River Valley." Several authors have described this unit from various perspectives, e.g. Sousa (1985), who studied the Corumbataí Formation and Estrada Nova facies in the state of São Paulo. It is Upper Permian in age and, according to its features, was formed in a platform environment with tidal influence, with input from the shallower-facies (lower shoreface) and deeper-facies associations (upper shoreface).

Materials and Methods

The research began with the elaboration of base maps for fieldwork purposes; these focused on the recognition of the lithofacies of the Corumbataí Formation in the area studied. The lithofacies identification was based on the methodology developed by Miall (1994). Detailed geological descriptions were given for 16 vertical profiles by means of data collection from mines in the area. Samples were collected and photographed in the field and then were sent to the laboratory for analyses as described below.

Granulometric analysis of ground samples was done by laser diffraction (Malvern Instruments Ltd, Malvern, Worcestershire, England), in which a sample aliquot, with particle size of <0.42 mm, was placed in a water solution and three drops of sodium hexametaphosphate (10%) added, obtained from the American House for Laboratory Articles (São Paulo, Brazil). The main methods of granulometric analysis in the control of ceramic raw materials were described by Orts et al. (1993). X-ray diffractometry was used to identify the mineral phases (Brindley & Brown, 1980; Thiry, 1974). The clay fraction was arranged on glass sheets (using preferred orientation) and analyzed after undergoing natural drying, solvation with ethylene glycol for 48 h, and heating in a muffle furnace at 500°C for 2 h. Mineralogical analyses were performed using a Panalytical X-ray diffractometer (Almelo, Netherlands). Measurements were made using CuKα_1 radiation ($\lambda = 1.54056$ Å) and a Ni filter. Interpretation of XRD traces and the semi-quantitative abundance of minerals were based on peak height using the Panalytical software *X'Pert HighScore Plus*.

For major elements s, a fraction of each of the samples was ground (to a diameter of ≤0.42 mm). The major elements were analyzed using inductively coupled plasma-atomic emission spectrometry (ICP-AES) by Labexchange (Baden-Württemberg, Germany). Loss on ignition (LOI) was measured by weight difference before and after combustion at 1000°C. The sample-preparation method used was fusion with lithium metaborate obtained from PGM Vectra (São Paulo, Brazil) (Penanes et al., 2022).

Following mineralogical, chemical, and granulometric analyses, ceramic characterization of the samples by the dry process was carried out under laboratory conditions. Initially, complete samples were crushed, divided into four, ground in a hammermill, moistened, pressed, and heated in a lab oven at 1050°C. This temperature was chosen for laboratory testing because it is close to the temperatures used commercially. After those procedures, tests were carried out for water absorption, apparent porosity, apparent density, linear firing and drying shrinkage, flexural strength module, and loss on ignition. All measurements followed the ABNT NBR–13818/1997 standards, and the results were sorted according to the water absorption group (Table 1).

Results

Geology and Lithofacies

The Corumbataí Formation crops out broadly in the area that has been studied (Fig. 1). In Porto Ferreira, this unit

https://doi.org/10.1007/s42860-022-00212-6 Published online by Cambridge University Press

Table 1 Classification of ceramic tiles according to ABNT (1997) applied to pieces 2 cm × 7 cm in size

Water absorption (%)	Flexural rupture module (kgf/cm^2)	Group ABS	Commercial nomenclature
0–0.5	300–500	BIa	Porcelain
0.5–3.0	300–450	BIb	Stoneware
3.0–6.0	320–350	BIIa	Semi-stoneware
6.0–10.0	180–300	BIIb	Semi-porous
10–20	150–200	BIII	Porous

occurs consistently throughout the city. The upper contact has mostly undifferentiated Cenozoic cover, and the bottom contact has tabular intrusions. In Tambaú, this unit presents the upper contact with the Botucatu Formation, and the lower contact with the Itararé Subgroup. This unit offers less exposure in Santa Rosa do Viterbo, and its upper contact has undifferentiated Cenozoic cover; its bottom contacts are tabular intrusions.

According to the facies survey, the lithofacies were grouped into lower shoreface and upper shoreface associations. The geological profiles studied, the lithofacies identified, and the sample locations are shown in Fig. 2.

Lower shoreface association. This facies association contains massive lithofacies at the bottom and laminated siltstone lithofacies on the top. (Fig. 3).

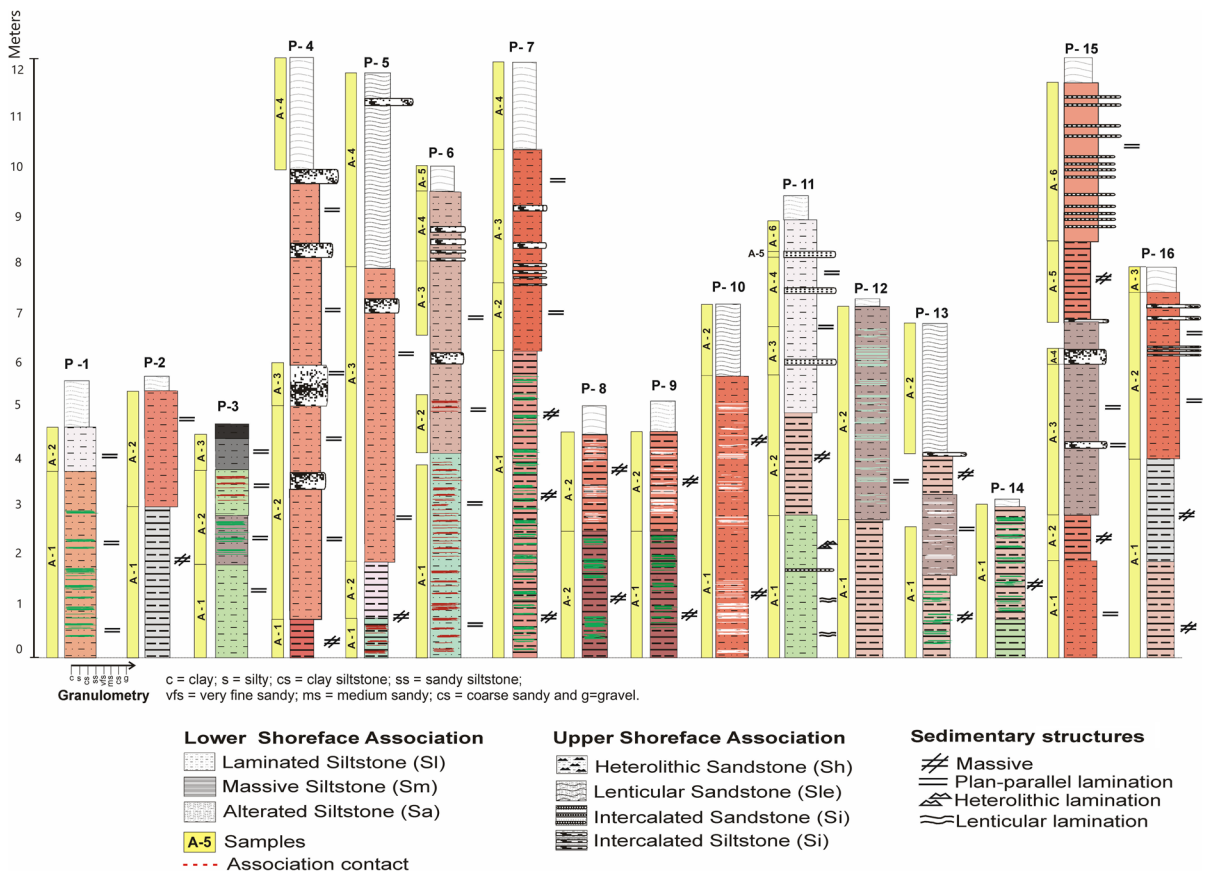

Fig. 2 Studied profiles in the study area. Thickness (m), granulometry, facies (associated colors and sedimentary structures present) and samples collected

https://doi.org/10.1007/s42860-022-00212-6 Published online by Cambridge University Press

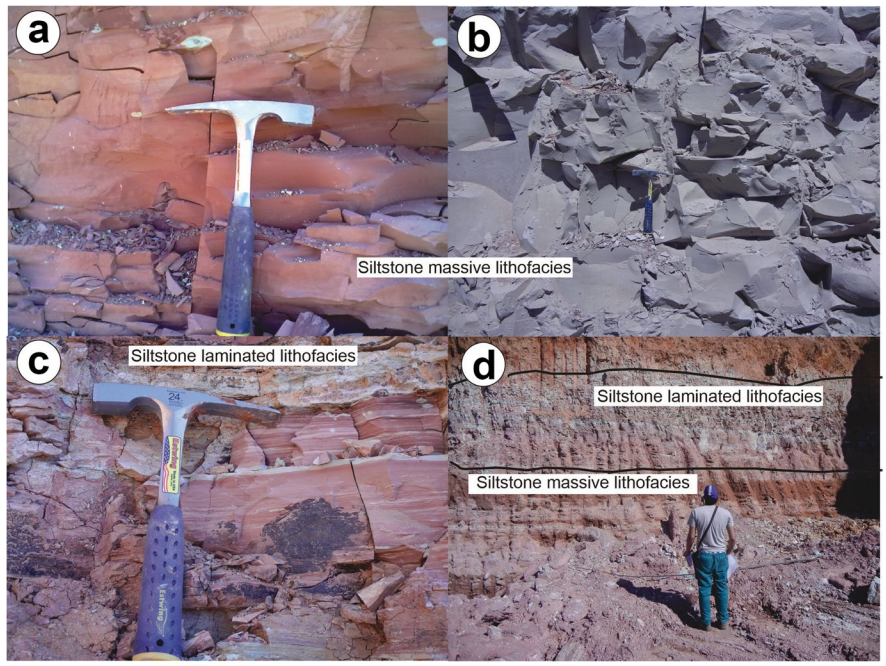

Fig. 3 Details of Lower Shoreface Association lithofacies: **a**,**b** massive siltstone lithofacies; **c** laminated lithofacies; and **d** contact between massive and laminated lithofacies

Massive siltstone (Sm): showing massive structure and gray, red, and purple coloration, forming beds with thicknesses ranging from 70 cm to ~5 m. The boundary between them is given by thin layers (up to 5 cm) of very-fine sandstone composed of quartz grains or by Bone beds, consisting of fragments of up to 6 mm of teeth and scales of *Palaeonisciformes* and bivalve shells of subclasses *Anomalodesmata*, *Pteriomorphia*, *Heterodonta*, and *Palaeoheterodonta* (Salvador & Simone, 2010).

Laminated siltstone (Sl): showing gray, red, and purple coloration, represented by massive siltstone showing millimetric laminations of whitish, very fine sand. Iron and manganese nodules can also be found.

Upper shoreface association: consisting from bottom to top of sandy-silty lithofacies, including heterolithic sandstone, lenticular sandstone, intercalated silty, and sandy. This association is dominated by an increase in the sand toward the tops of sections.

Heterolithic sandstone (Sh): is characterized by fine, silty sandstone intercalations, with green pelitic blades, forming mud couplets. The sandstone presents well-sorted grains; rounded with reddish beige coloring, and strata with thicknesses ranging from 1 to 15 cm. They present planar-parallel stratification and wavy marks with drapes of clay. Concentrations of manganese nodules up to 2 cm in diameter are common, as well as shafts of silicon carbonate composition discordant with bedding (Fig. 4).

Lenticular sandstone (Sle): consists of reddish-brown pelitic deposits with lenses from very fine to fine sandstone, well-sorted grains, 1.5 m long, with a thickness of up to 15 cm, and lenticular cross-stratification. In addition, it has irregular horizontal tubes, 1 cm in diameter, filled with very fine sandstone, which can be found at some sites. Sandstones can often form layers tens of meters long and up to 30 cm thick. It also has sole marks on the bottom and steep top (Fig. 5). Commonly, these lithofacies are repeated above the sandy facies at the tops of the units.

Intercalated sandstone/siltstone (Si): this lithofacies occurs either with sand prevailing over the clay (sandy intercalated lithofacies) or clay over the sand (silty intercalated lithofacies). Sandstone and siltstone layers feature varying centimeter thicknesses and can be referred to as 'rhythmite' (Fig. 6a,b).

Altered siltstone (Sa): altered without preserved sedimentary structures, it has white, light red, and yellowish colors, the superficial part of the profiles.

https://doi.org/10.1007/s42860-022-00212-6 Published online by Cambridge University Press

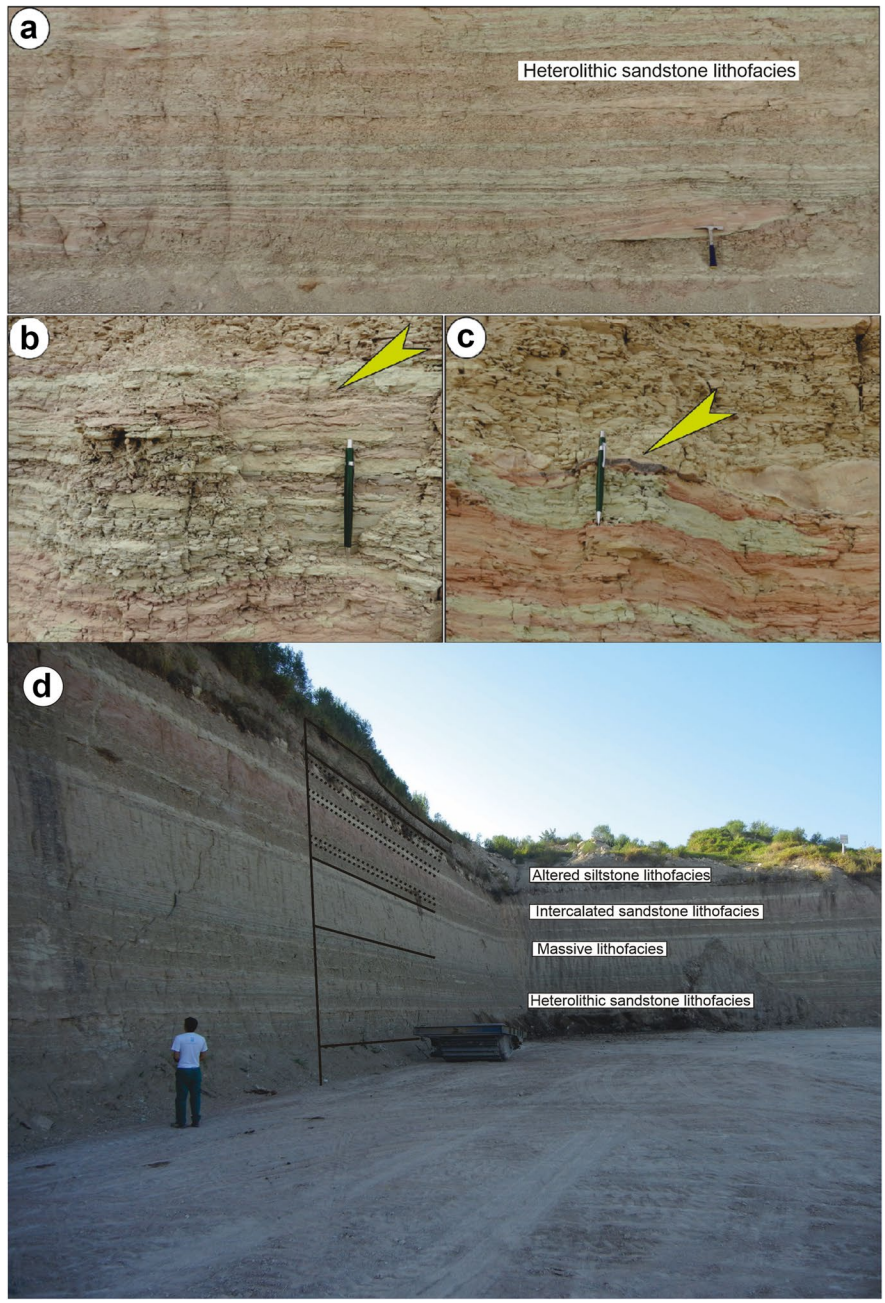

Fig. 4 **a** Heterolithic sandstone lithofacies, outcrop exposing (at the bottom) reddish-brown pelite overlapped by thin sandstone intercalations, well-sorted grains with greenish gray claystones (cut and fill). At the top is fine sandstone with planar-parallel, wavy, and clay drapes. **b** Close-up of the conjugated pairs of clay (mud couplets). **c** Close-up of manganese dioxide concentration and **d** P11 profile

Granulometry

The granulometric distribution of dry-ground samples was analyzed by laser diffraction (Fig. 7). Multimodal behavior was observed in diagrams at various granulometric tracks. The largest concentrations of particles are in the intervals 1–10 μm and 10–100 μm, with mean values ranging from 48.23 to 73.03% and

https://doi.org/10.1007/s42860-022-00212-6 Published online by Cambridge University Press

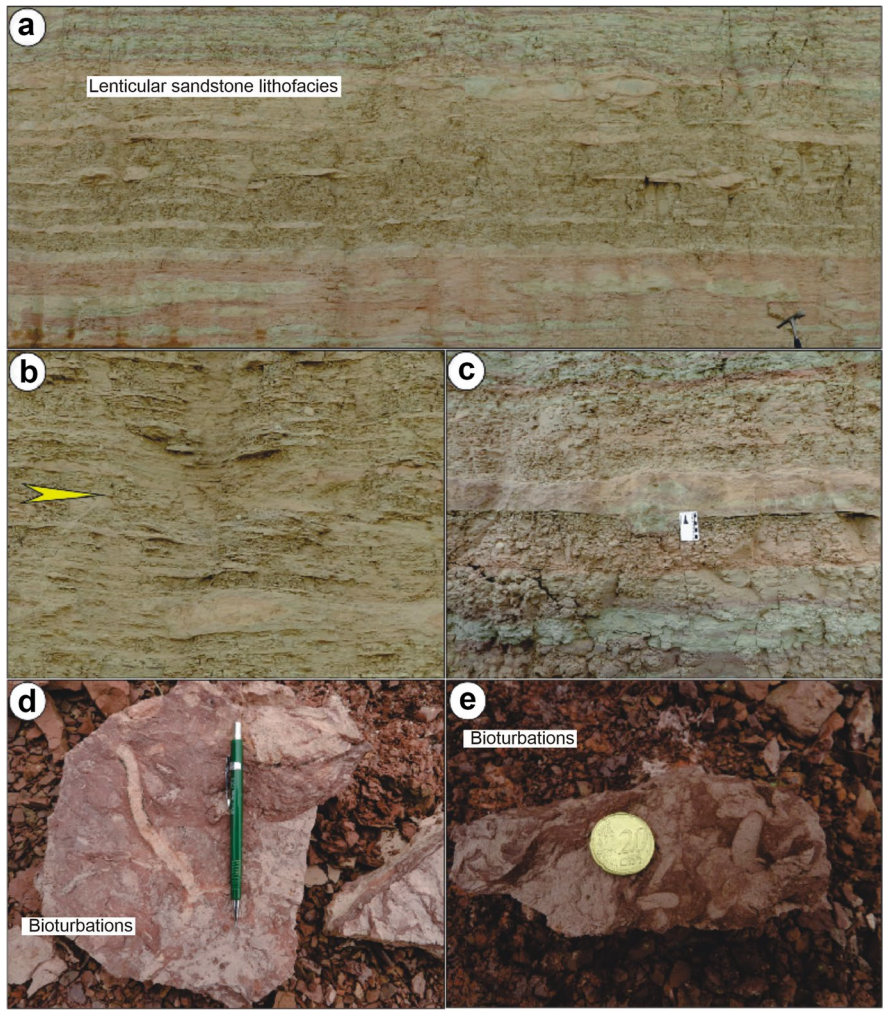

Fig. 5 Lenticular sandstone lithofacies. **a** Mudstones and sandstones with cross lenticular stratification; **b** Close-up of lenticular sandstone (yellow arrow indicates the direction of the paleochannel); **c** Sandstone layers with sole marks at the bottom and steep top. **d**,**e** Bioturbations filled with very fine sandstone

from 20.70 to 38.26%, respectively (Table 2, Fig. 7), classified, according to Wentworth (1922), as thick siltstone to very fine sandstone. Smaller percentages of grains are distributed in intervals which are 0.1–1 μm and 100–1000 μm in most of the studied sections; but when the distribution is less well sorted and there are grain concentrations in these intervals, there is an improvement in the ceramic properties, as can be seen in the samples of profiles P7 and P15. This happens because of the packing of particles during the pressing process which favors sintering and thus improves the ceramic properties.

Mineralogy

The mineralogical composition is illustrated in Table 3 and Fig. 8. Among the minerals present were as follows. (1) A group of silicates; quartz occurred in all XRD traces of the whole rocks, with its principal peak at $d_{001} = 3.33$ Å; two types of feldspar – microcline and albite – microcline was more abundant, with $d_{001} = 3.24$ Å. (2) Non-silicate minerals; calcite and dolomite, were identified in the whole-rock sample; calcite was found in most of the profiles studied and showed a its main peak at $d_{001} = 3.00$ Å. In the P5, P7,

https://doi.org/10.1007/s42860-022-00212-6 Published online by Cambridge University Press

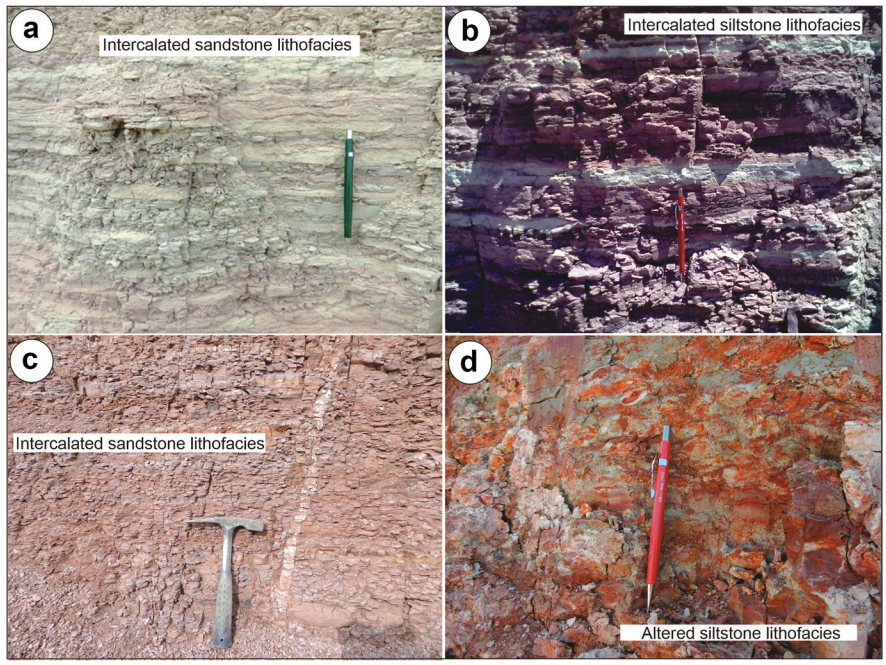

Fig. 6 **a,b** Intercalated siltstone lithofacies; **c** intercalated sandstone lithofacies; and **d** altered siltstone lithofacies

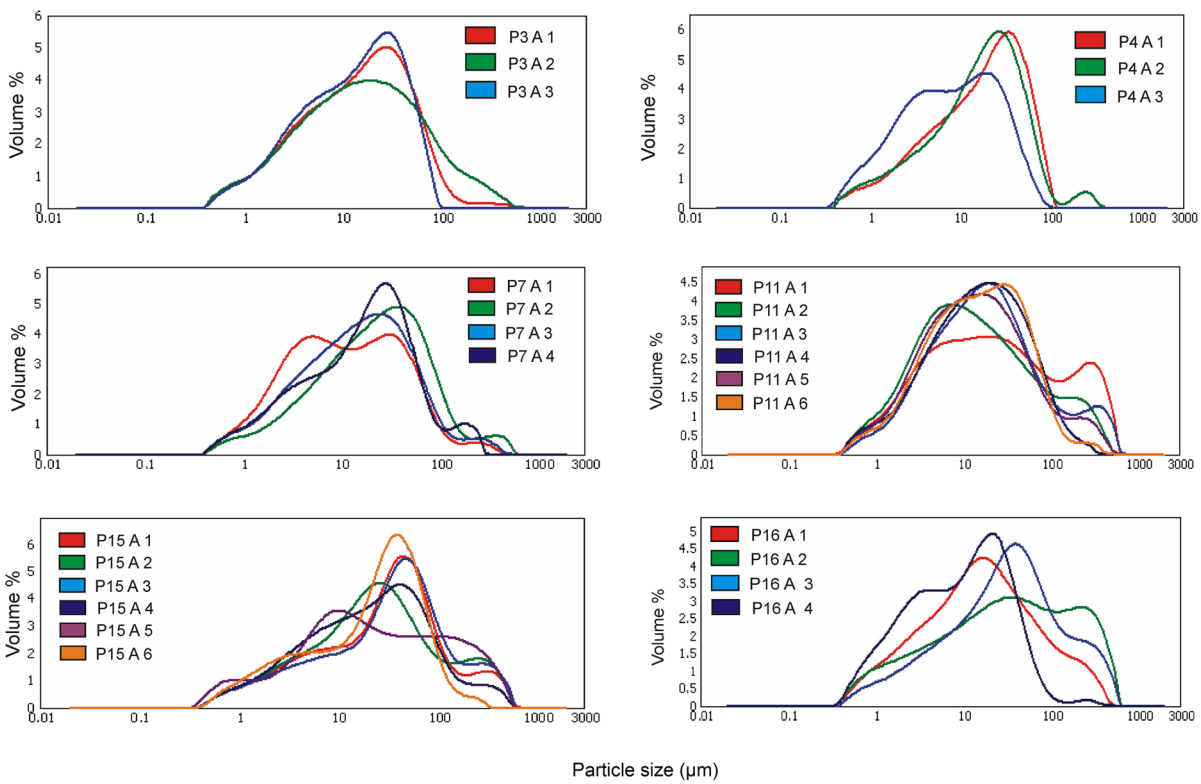

Fig. 7 Laser granulometric distribution of the P3, P4, P7, P11, P15, and P16 profiles

https://doi.org/10.1007/s42860-022-00212-6 Published online by Cambridge University Press

Table 2 Granulometric distribution by laser diffraction (%)

Samples	0.1–1 µm	1–10 µm	10–100 µm	100–1000 µm
P1-A1	3.048	31.58	65.37	0.00
P1-A2	2.467	19.73	64.51	13.29
Average	2.75	25.65	64.94	6.64
P2-A1	6.57	37.84	55.59	0.00
P2-A2	5.78	31.70	61.7	0.81
Average	6.17	34.77	58.64	0.40
P3-A1	4.11	36.62	57.13	2.13
P3-A2	4.17	36.83	50.93	8.07
P3-A3	3.959	39.71	56.25	0.00
Average	4.08	37.75	54.77	3.4
P4-A1	3.18	29.00	58.56	8.47
P4-A2	3.74	29.48	58.7	8.47
P4-A3	8.29	50.15	41.8	0.00
Average	5.07	36.21	53.02	5.64
P5-A1	4.15	25.42	67.71	2.71
P5-A2	4.31	30.63	62.69	2.37
P5-A3	5.455	35.53	59.01	0.00
Average	4.64	30.53	63.13	1.69
P6-A1	3.93	31.06	61.12	3.88
P6-A2	2.58	25.30	70.80	1.31
P6-A3	4.00	28.21	65.23	2.55
P6-A4	3.55	24.95	69.77	1.73
P6-A5	6.12	37.21	56.58	0.08
Average	4.03	29.35	64.7	1.91
P7-A00	4.24	46.6	46.07	3.09
P7-A1	2.77	28.46	61.31	7.45
P7-A2	4.01	37.11	54.45	4.43
P7-A3	3.89	32.75	58.22	5.13
Average	3.73	36.23	55.01	5.02
P8-A1	3.78	35.42	51.10	9.69
P8-A2	3.34	31.76	63.34	1.65
Average	3.56	33.59	57.22	5.67
P9-A1	5.34	25.20	67.16	2.29
P9-A2	3.17	22.02	73.23	1.57
P9-A3	4.50	40.34	55.04	1.12
Average	4.33	29.19	65.14	1.66
P10-A1	3.18	28.65	66.96	1.2
P10-A2	4.40	43.00	52.6	0.00
Average	3.79	35.82	59.78	0.6
P11-A1	3.13	24.77	58.80	12.79
P11-A2	3.01	27.04	52.74	15.93
P11-A3	3.25	22.14	58.21	16.96
P11-A4	3.09	30.8	57.04	10.00
P11-A5	5.25	30.7	42.80	5.25
P11-A6	3.57	27.1	64.86	3.57
Average	3.55	27.09	55.74	10.75
P12-A1	5.213	35.63	55.63	3.52
P12-A2	3.382	26.72	65.11	4.78
Average	4.29	31.18	60.37	4.15
P13-A1	2.69	23.39	67.95	5.96
P13-A2	2.22	18.02	78.11	1.65
Average	2.45	20.70	73.03	3.80
P14-A1	3.68	38.18	51.49	6.65
P15- A1	3.54	35.47	38.06	23.38
P15-A2	4.48	43.16	41.12	11.24
P15-A3	2.64	33.37	52.62	11.30
P15-A4	4.01	37.06	55.69	3.23
P15-A5	3.70	41.29	47.36	7.68
P15-A6	3.13	39.24	54.72	2.91
Average	3.58	38.26	48.26	9.96
P16-A1	4.92	35.74	49.35	9.98
P16-A2	5.25	25.45	43.74	25.55
P16-A3	3.02	22.97	56.11	17.89
P16-A4	7.7	44.92	46.31	1.07
Average	5.22	32.27	48.87	13.62

P11, and P16 profiles (Fig. 8) associated with calcite, the dolomite mineral occurs with greater intensity at d_{001} = 2.88 Å. In the oxides – where hematite was prominent in samples of the P4 profile, with a notable peak at d_{001} = 2.69 Å, magnetite also occurred, but less frequently, with the main peak at d_{001} = 2.53 Å. (3) A group of clay minerals, where illite, kaolinite, and montmorillonite were prevalent, their structure (phyllosilicates) allowed preferred orientation in the fine fraction, revealing prominently the peaks for d_{001}, d_{002}, and d_{003}. The most abundant clay mineral in the Corumbataí Formation is illite, found in all studied profiles, with interlayer spacing (d_{001}) of 10 Å in natural conditions. This did not change when subjected to heating (500°C) and treatment with ethylene glycol, maintaining a peak of 10 Å. Peaks representing d_{002} at 4.98 Å and d_{003} at 3.32 Å were also noted.

Kaolinite and montmorillonite exchange places as the second most abundant mineral in the profiles studied. Kaolinite occurred as the most abundant clay mineral in samples P1-A2 and P4-A3, predominantly in the upper strata. It has a d_{001} spacing of 7 Å in the natural condition, and when subjected to heat (500°C), the peak vanished. The d_{002} is at 3.58 Å, and

https://doi.org/10.1007/s42860-022-00212-6 Published online by Cambridge University Press

the d_{003} at 4.36 Å. On the other hand, the clay mineral of the smectite group identified was montmorillonite, present with greater prominence in samples of the P3 and P15 profiles (Table 3, Fig. 8), showing $d_{001} = 14.8$ Å, and when subjected to treatment with ethylene glycol, its value shifted to 17 Å.

Chemical

The major elements percentages and respective averages are listed in Table 4. SiO_2 represents the most prevalent oxide in the studied sections, with average values of 65.01%, and MnO is the least abundant, with 0.05%. According to the oxides diagrams, shown in Fig. 9 (Rollinson, 1995), we have observed that when with increasing SiO_2, Al_2O_3 tends to decrease. It occurs due to the loss of SiO_2 in the upper layers by the alteration process of the feldspar and the clay minerals illite and montmorillonite. On the other hand, Fe_2O_3, TiO_2, and LOI increased when Al_2O_3 increased. Alkali oxides (K_2O, Na_2O) and alkaline earth metals (MgO and CaO) varied irregularly with increasing Al_2O_3. The average values of SiO_2 were between 60 and 70% (Fig. 9, Table 4), and the greatest concentration was found in sample P16-A2, with 77.57%, and the lowest, 49.36%, found in sample P11-A5. The overall average amount of Al_2O_3 was 14.29%, with greater average values in the P4 profile of 18.60%; the lowest values of 10.63% were in the P11 profile (Table 4). Al_2O_3 and SiO_2 are considered to be refractory elements.

K (in illite) and Na (in albite) are responsible for sintering. Their average contents, expressed in oxide form, were 0.20% (Na_2O) and 3.39% (K_2O). These elements and MgO (2.00%) did not correlate well with increasing Al_2O_3, revealed by the scattered points (Fig. 9); this was probably the result of mixed sources (minerals) and distinct behavior; another major source of K_2O is the mineral feldspar. Both feldspar and illite tend to evolve into kaolinite; on the other hand, Mg is found in minerals such as illite, chlorite, and carbonates, as the main element or substituted for other elements with similar ionic behaviors. For Na, most samples have small concentrations; it is found in albite and montmorillonite and as a substitute for other elements, such as mineral crystals of Ca and K (Rollinson, 1995).

The largest relative amount of CaO was found in the P11 profile, with 5.84% on average, and the smallest in the P4 profile, with a value of 0.05%. This element stood out in samples P11-A2, P11-A5, and P16-A3, with 8.81, 21.41, and 9.13%, respectively. Greater amounts of MgO were found in samples of the P15 profile, with values of 2.85% and smaller values of 0.56% in the P2 profile. More Na_2O (0.41%) was present in the P15 profile and less (0.05%) in the P13 profile; this is a very small amount compared to the levels found in the Corumbataí Formation in the Santa Gertrudes ceramic region. K_2O made up 6.10% in the P15 profile and 0.90% in P10 profile. Profiles that showed greater percentages of MgO were P11 and P15, and the value in sample P11-A2 was 4.84%.

The sum of $CaO + Na_2O$ (Fig. 10c) was 0–3% in all samples except P11-A5, which had a value of 21.59%. A reverse trend was observed between SiO_2 concentration and the sum of $Al_2O_3 + TiO_2 + Fe_2O_3$ (Fig. 10a). The largest differences occurred in samples P11, P11-A2, and P11-A5 due to the small amount of SiO_2 and the high percentages of CaO confirmed in the XRD patterns (Fig. 8). In the P16 profile, sample P16-A2 contained the most SiO_2 (77.57%), also confirmed by the highest quartz peak in XRD (Fig. 8). The other elements, P_2O_5, MnO, and TiO_2, were present in smaller amounts.

Ceramic Properties

To identify the ceramic properties, tests were performed on samples of the studied sections (Table 5). The use of clayey raw materials in tile manufacturing depends on the technological and appearance requirements of the ceramic body, such as color after firing and behavior of the masse during the tile-making process; both properties are related intimately to mineral composition, chemical composition, and particle-size distribution (Dondi, 1999).

Of sixteen profiles, ten representative profiles were selected for ceramic testing, having been evaluated for the following features: flexural strength, water absorption, apparent porosity, apparent dry density, shrinkage upon linear firing, and granulometric distribution by laser diffraction. Thirty-nine samples were analyzed and classified according to their water absorption group (Table 5): 22 (56.4%) in Group BIII (porous); six (15.4%) within Group BIIb (semi-porous); two (5.12%) in BIIa (semi-stoneware); eight (20.5%) in Group BIb (stoneware) and one (2.6%) in Group BIa (porcelain). The overall average water-absorption percentage for all

https://doi.org/10.1007/s42860-022-00212-6 Published online by Cambridge University Press

Table 3 Relative quantification (by XRD) of minerals present. Obs. 15 Å (montmorillonite), 10 Å (illite), 7 Å (kaolinite), 4.26 Å (quartz), 3.24 Å (microcline), 3.19 Å (albite), 3.00 Å (calcite), 2.88 Å (dolomite), and 2.69 Å (hematite)

	H_{rel} (relative height)								
Samples	15 Å	10 Å	7 Å	4.26 Å	3.24 Å	3.19 Å	3.00 Å	2.88 Å	2.69 Å
P1-A1	**	****	*	***	**				***
P1-A2		**	***	***	****				*
P2-A1	*	*	**	***			**		*
P2-A2		*	**	****			*		
P3-A1	***	*		***	**		**		
P3-A2	**	**		***	***		**	*	*
P3-A3	****	*		**	**		**	*	
P4-A1		***	**	**	*	*	*		****
P4-A2		***	*	**	***	****	**		**
P4-A3		***	****	***			*		****
P5-A1		***	*	***	****	***	***	***	
P5-A2		****		**	***		**	*	
P5-A3		****		*	****		**	***	*
P5-A4		***	**	*					***
P6-A1		***		***	***		**	*	
P6-A2	*	**		*	***		**		
P6-A3		***		***	*		*		
P6-A4		**	**	***	**				*
P6-05		***	**	**			*		**
P7-A1		**		*	*		*		*
P7-A2	****	*	**	***	**	*	*		
P7-A3	*	*		**	*				
P7-A4	*	*		**	*		**		
P8-A1	**	*		**	**	***	*	*	**
P8-A2	*	**		**	**		*		**
P9-A1		*		**	***	*	**	***	
P9-A2		**		***	***		**		
P9-A3		**		**	*		*	*	
P10-A1	**	**		**	*		*		**
P10-A2		****		*	*				
P11-01		**	*	**	**	***	**	**	
P11-A2		**		*	**	*	***	****	**
P11-A3		*		**	**	*	**	**	
P11-A4		***		**	**	***	*	*	
P11-A5	*	*		*	*		****	*	**
P11-A6		***		*	***	**	**	**	
P12-A1		***		**	**		*	*	
P12-A2		**		**	**		*		
P13-A1		***	*	*	*		*	*	*
P13-A2			*	*	*			*	*
P14-A1	*	**		**	*		*		
P15-A1	*	***	*	**	*	**	*		**
P15-A2	**	***	*	**		**	*		**

https://doi.org/10.1007/s42860-022-00212-6 Published online by Cambridge University Press

Table 3 (continued)

Samples	H_{rel} (relative height)								
	15 Å	10 Å	7 Å	4.26 Å	3.24 Å	3.19 Å	3.00 Å	2.88 Å	2.69 Å
P15-A3	*	*	*	**		*	*		**
P15-A4	****	*		**		*			*
P15-A5	**	***		**	**	**	*		***
P15-A6	***	***		**	***	**	*		**
P16-A1	***	***		****	**	**	**		
P16-A2	*	***		*	*		***	*	**
P16-A3	**	***		*	**	**	****	**	
P16-A4	***	**	**	**			*		*

Frequency: * (very low), ** (low), *** (medium), **** (high)

samples was 9.75%, which falls within the Group BIIb classification, and the average flexural strength was 245 kgf/cm^2. Samples from the P1, P2, P3, P4, P11, and P16 profiles are classified in Group BIII and the P6 profile in Group BIIb. The P6 and P15 profiles gave the best ceramic results, with average flexural rupture modulus (MRF) values of 323.52 kgf/cm^2 and 345.48 kgf/cm^2 and water absorption (WA) of 5.88% and 4.10%.

Discussion of Results

Based on the results obtained, the Corumbataí Formation, other than samples P6, P7 and P15, shows similar geological, mineralogical, chemical, and ceramic characteristics to the profiles studied. The facies study allowed the lithofacies identified to be grouped into two facies associations: Lower Shoreface Association and Upper Shoreface Association. In the Lower Shoreface Association, the lithofacies found were massive siltstone (Sm) and laminated siltstone (Sl). According to Sousa (1985), the characteristics indicated sedimentation by settling in a marine-platform environment, below the level of waves and low-energy waves. In the Upper Shoreface Association, the lithology consisted, from bottom to top, of heterolithic sandstone (Sh), lenticular sandstone (Sle), and intercalated siltstone/sandstone (Si) lithofacies. In this association, an increase in sand and energy prevailed towards the top of the profiles, reflecting directly the mineral and chemical composition and the ceramic properties found.

According to mineralogical identification by XRD, the main minerals present belong to the following mineral groups: tectosilicates, carbonates, oxides, and phyllosilicates. The tectosilicate is the most abundant mineral group in rocks of the Corumbataí Formation and is represented mainly by quartz and feldspars (microcline and albite). The dominant feldspar type in the studied samples differed from that found in the Santa Gertrudes Ceramic cluster region, however. In the studied area, microcline is predominant, while in the Ceramic cluster region, albite is more frequent (Christofoletti et al., 2006).

Thus, potassium is the element that could contribute most to the formation of a liquid phase during firing as it is found in illite which releases this element at low temperatures; potassium feldspar remains in the firing processes virtually unchanged. The carbonates (calcite and dolomite) and oxides (represented by hematite) are lessfrequent. The calcite and dolomite increase the porosity and decrease the mechanical resistance, as can be observed in samples P11-A2, P11-A5, and P16-A3.

Regarding phyllosilicates, illite is predominant, followed by kaolinite and montmorillonite. Illite occurs in the basal and intermediate portions with kaolinite and smectite in the upper portions, sometimes in the form of alterites. The geochemical results obtained by quantifying the major elements confirm the mineralogy found. SiO_2 is the most prevalent element and is found in the form of quartz, feldspar, and phyllosilicates. K_2O is in the composition of the microcline feldspar and the composition of illite.

According to the ceramic results, almost all studied samples were classified within the BIII group of water absorption as 'porous,' with water absorption values of between 10 and 20% and modulus of rupture at between 150 and 200 kgf/cm^2. This is due to low concentrations of Na_2O, the significant amount of microcline, and coarser granulometry identified in fieldwork

https://doi.org/10.1007/s42860-022-00212-6 Published online by Cambridge University Press

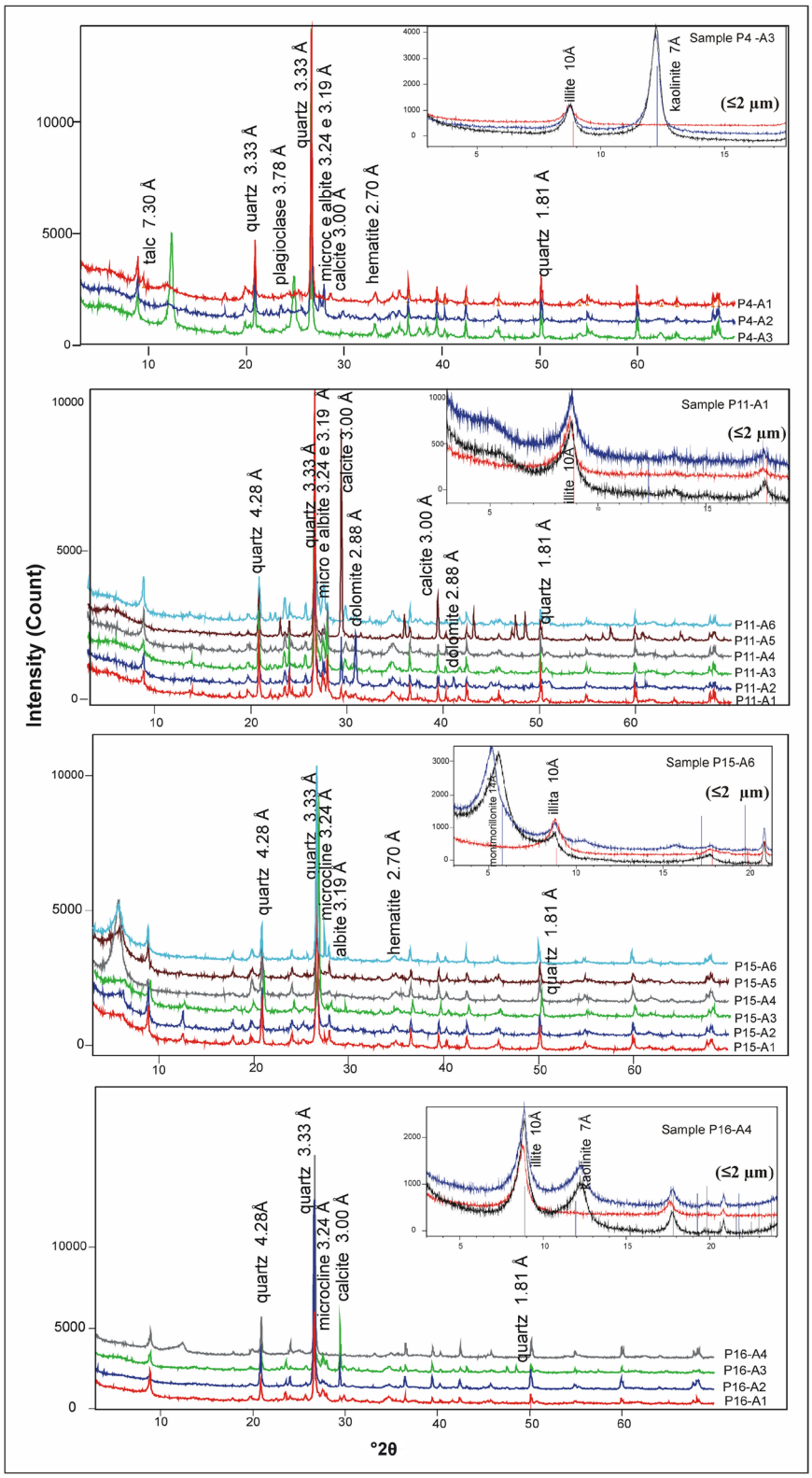

Fig. 8 XRD of whole-rock samples with clay fractions inset

https://doi.org/10.1007/s42860-022-00212-6 Published online by Cambridge University Press

Table 4 Chemical composition, obtained by ICP-MS, of the major elements (%)

Samples	Al_2O_3	CaO	TiO_2	SiO_2	Fe_2O_3	K_2O	MgO	MnO	Na_2O	P_2O_5	LOI	Sum
P1-A1	16.26	0.28	0.70	62.39	5.09	2.01	1.87	0.07	0.06	0.06	6.28	95.07
P1-A2	13.75	0.07	0.63	72.41	2.92	1.09	0.83	0.08	0.05	0.02	4.98	96.83
Average	15.00	0.17	0.66	67.4	4.00	1.55	1.35	0.07	0.05	0.04	5.63	
P2-A1	15.51	0.02	0.63	65.65	5.92	0.99	0.45	0.02	0.03	0.03	5.87	95.12
P2-A2	12.28	0.01	0.55	72.84	4.41	0.82	0.67	0.02	0.04	0.01	4.53	96.18
Average	13.89	0.01	0.59	69.24	5.16	0.90	0.56	0.02	0.03	0.02	5.20	
P3-A1	13.84	0.51	0.56	70.02	4.12	2.2	1.42	0.01	0.09	0.06	5.53	98.36
P3-A2	12.72	0.4	0.53	68.51	4.87	3.83	1.97	0.02	0.14	0.05	4.32	97.36
P3-A3	13.88	0.6	0.64	70.69	2.32	2.35	2.03	0.02	0.07	0.04	5.59	98.23
Average	13.48	0.50	0.57	69.74	3.77	2.80	1.80	0.01	0.1	0.05	5.14	
P4-A1	18.66	0.04	0.89	58.53	6.76	1.63	2.62	0.18	0.04	0.03	6.92	96.30
P4-A2	17.35	0.11	0.72	62.52	5.1	3.00	1.33	0.1	0.88	0.04	5.07	96.22
P4-A3	19.81	0.01	0.89	57.73	7.12	1.53	0.61	0.07	0.07	0.15	7.05	95.04
Average	18.60	0.05	0.83	59.60	6.33	2.0	1.52	0.11	0.33	0.07	6.34	
P5-A1	12.69	0.17	0.44	67.07	2.87	7.94	1.46	0.03	0.39	0.04	2.04	95.14
P5-A2	13.89	0.17	0.56	64.03	4.15	7.98	2.15	0.06	0.19	0.02	2.84	96.04
P5-A3	13.72	0.12	0.53	63.61	4.78	6.55	2.28	0.18	0.17	< 0.01	3.71	95.66
P5-A4	16.41	0.06	0.62	64.61	5.39	1.95	1.35	0.04	0.04	0.01	5.89	96.37
Average	14.17	0.13	0.53	64.83	4.29	6.10	1.81	0.07	0.19	0.02	3.62	
P6-A1	15.03	0.13	0.55	64.74	4.25	5.05	2.54	0.07	0.13	0.04	4.83	97.36
P6-A2	16.41	0.07	0.55	62.24	4.19	3.53	2.94	0.05	0.11	0.06	6.47	96.62
P6-A3	16.25	0.02	0.60	63.05	4.35	3.37	2.6	0.03	0.06	0.07	5.85	96.25
P6-A4	16.81	0.02	0.51	63.83	3.63	2.35	1.88	0.03	0.08	0.04	6.64	95.82
P6-A5	15.48	0.02	0.71	61.2	6.14	3.55	2.42	0.04	0.06	0.03	5.82	95.47
Average	15.99	0.05	0.58	63.01	4.51	3.57	2.47	0.04	0.08	0.04	5.92	
P7-A1	14.83	0.38	0.58	61.2	5.25	4.76	3.04	0.02	0.11	0.03	5.17	95.37
P7-A2	11.92	0.83	0.35	70.37	2.62	2.42	2.61	0.04	0.25	0.04	5.83	97.28
P7-A3	14.56	0.43	0.58	62.93	4.64	3.35	2.83	0.08	0.09	0.09	6.01	95.59
P7-A4	13.44	0.2	0.53	65.30	5.96	2.06	1.79	0.02	0.07	0.08	5.09	94.54
Average	13.68	0.46	0.39	64.95	4.61	3.14	2.56	0.04	0.13	0.06	5.52	
P8-A1	13.09	0.54	0.53	64.35	4.74	4.66	2.78	0.08	0.33	0.03	4.51	95.64
P8-A2	14.98	0.44	0.54	64.76	4.34	2.42	2.44	0.05	0.09	0.05	6.49	96.60
Average	14.03	0.49	0.53	64.55	4.54	3.54	2.61	0.06	0.21	0.04	5.50	
P9-A1	11.47	0.30	0.37	69.85	2.80	6.80	1.46	0.13	0.41	0.11	2.24	95.94
P9-A2	13.15	0.09	0.50	67.30	3.57	5.82	1.7	0.08	0.23	0.05	3.64	96.13
P9-A3	14.63	0.06	0.68	62.04	5.08	4.66	2.69	0.08	0.10	0.03	5.02	95.07
Average	13.08	0.15	0.52	66.40	3.81	5.76	1.95	0.097	0.24	0.06	3.63	
P10-A1	13.55	0.41	0.51	66.27	3.51	2.8	2.63	0.05	0.08	0.06	5.73	95.6
P10-A2	14.09	0.08	0.66	63.68	5.57	3.39	2.61	0.05	0.05	0.04	5.34	95.6
Average	13.82	0.24	0.58	64.97	4.54	3.09	2.62	0.05	0.06	0.05	5.53	
P11-A1	11.28	2.32	0.48	65.10	3.22	5.69	2.24	0.03	1.01	0.22	3.84	95.43
P11-A2	9.83	8.81	0.37	51.73	3.19	5.58	4.84	0.1	0.69	0.09	12.02	97.25
P11-A3	12.47	1.50	0.46	65.61	3.21	7.2	2.05	0.03	0.91	0.19	3.18	96.81
P11-A4	12.56	0.47	0.50	64.65	4.08	6.96	2.50	0.05	0.84	0.10	2.73	95.44
P11-A5	3.97	21.41	0.15	49.36	1.46	2.18	1.03	0.10	0.18	0.03	18.43	98.30

https://doi.org/10.1007/s42860-022-00212-6 Published online by Cambridge University Press

Table 4 (continued)

Samples	Al_2O_3	CaO	TiO_2	SiO_2	Fe_2O_3	K_2O	MgO	MnO	Na_2O	P_2O_5	LOI	Sum
P11-A6	13.71	0.57	0.51	64.24	3.75	8.14	2.16	0.04	0.88	0.13	2.31	96.44
Average	10.63	5.84	0.42	60.11	3.15	5.95	2.47	0.05	0.75	0.12	7.08	
P12-A1	12.98	0.14	0.44	66.27	3.77	5.17	2.38	0.07	0.25	0.04	4.19	95.70
P12-A2	18.08	0.07	0.49	60.15	3.99	2.99	2.49	0.10	0.09	0.09	6.86	95.40
Average	15.53	0.10	0.46	63.21	3.88	4.08	2.43	0.08	0.17	0.06	5.52	
P13-A1	18.65	0.03	0.54	60.83	3.89	2.30	1.62	0.02	0.09	0.04	7.20	95.21
P13-A2	13.69	0.02	0.46	72.94	2.29	0.89	1.14	0.02	0.02	0.10	5.23	96.80
Average	16.17	0.02	0.50	66.88	3.09	1.59	1.38	0.02	0.05	0.07	6.21	
P14-A1	15.21	0.22	0.62	64.43	4.76	2.75	1.96	0.02	0.07	0.10	5.68	95.82
Average	15.21	0.22	0.62	64.43	4.76	2.75	1.96	0.02	0.07	0.10	5.68	
P15-A1	13.25	0.73	0.53	69.26	4.38	2.96	2.99	0.04	0.61	0.19	3.93	98.87
P15-A2	14.76	0.45	0.67	62.71	5.04	3.12	3.33	0.04	0.64	0.06	4.62	95.44
P15-A3	13.69	2.29	0.54	62.60	4.75	2.92	3.17	0.05	0.47	1.05	4.61	96.14
P15-A4	12.67	0.85	0.30	69.60	3.40	1.61	2.72	0.03	0.36	0.07	5.68	97.29
P15-A5	14.96	0.63	0.65	62.31	6.04	3.27	3.21	0.07	0.40	0.11	4.94	96.59
P15-A6	14.26	0.73	0.59	66.57	4.17	2.68	2.57	0.04	0.33	0.11	5.06	97.11
Average	14.11	0.84	0.54	65.35	4.65	2.75	2.85	0.04	0.41	0.24	4.93	
P16-A1	12.82	1.56	0.50	64.09	4.05	7.16	2.96	0.05	0.58	0.1	3.72	97.59
P16-A2	6.49	2.51	0.24	77.57	2.27	3.71	1.57	0.03	0.21	0.09	3.40	98.09
P16-A3	10.68	9.13	0.37	55.18	3.08	6.25	2.36	0.06	0.55	0.11	9.20	96.97
P16-A4	15.61	0.05	0.53	65.34	4.53	1.82	1.3	0.06	0.03	0.04	5.92	95.23
Average	11.4	3.31	0.46	65.54	3.48	4.73	2.04	0.05	0.34	0.08	5.56	
Total Average	14.29	0.79	0.55	65.01	4.28	3.39	2.00	0.05	0.20	0.63	5.43	

and confirmed by laser diffraction granulometry. These allied factors resulted in a greater porosity of the fired pieces, resulting in poor packaging during pressing, limiting the reactivity between the grains.

In profiles P6, P7, and P15, the ceramic results differ from the others that have been studied, with most samples classified within the BIIb and BIb Groups (semi-porous and stoneware). The ceramic properties of the P15 profile were similar to those obtained from the raw materials found in the Santa Gertrudes Ceramic Cluster, such as the red color, finer granulometry, and a better distribution of grains, favored by the greater concentration of clay minerals. This may be related to the proximity of a heat source – the basic intrusions resulting from the action of Serra Geral basaltic magmatism of Cretaceous age (Costa, 2006).

Conclusions

The major outcomes of this study can be summarized as follows:

(1) the results obtained here expand the scientific knowledge of the Corumbataí Formation from the geological, mineralogical, chemical, and ceramic properties points of view. This information is critical to a better understanding of the same rocks in other locations as source materials, and is fundamental to the sustainability of the ceramic-coating industry in the State of São Paulo.

(2) The ceramic behavioral trends of the six facies identified and studied are similar to those in the Corumbataí Formation in the Santa Gertrudes Ceramic Cluster where the vertical succession or stacking comprises an ascending grain growth, with a predominance of finer/clayey pelitic facies at the base (massive and laminated), evolving to predominantly coarser/sandier lithofacies interspersed with pelitic facies on top (heterolithic, lenticular, and intercalated). These facies indicate sedimentary processes typical of a shelf marine environment, below the average level of normal waves and dominated by tidal flows. The increase in the sand

https://doi.org/10.1007/s42860-022-00212-6 Published online by Cambridge University Press

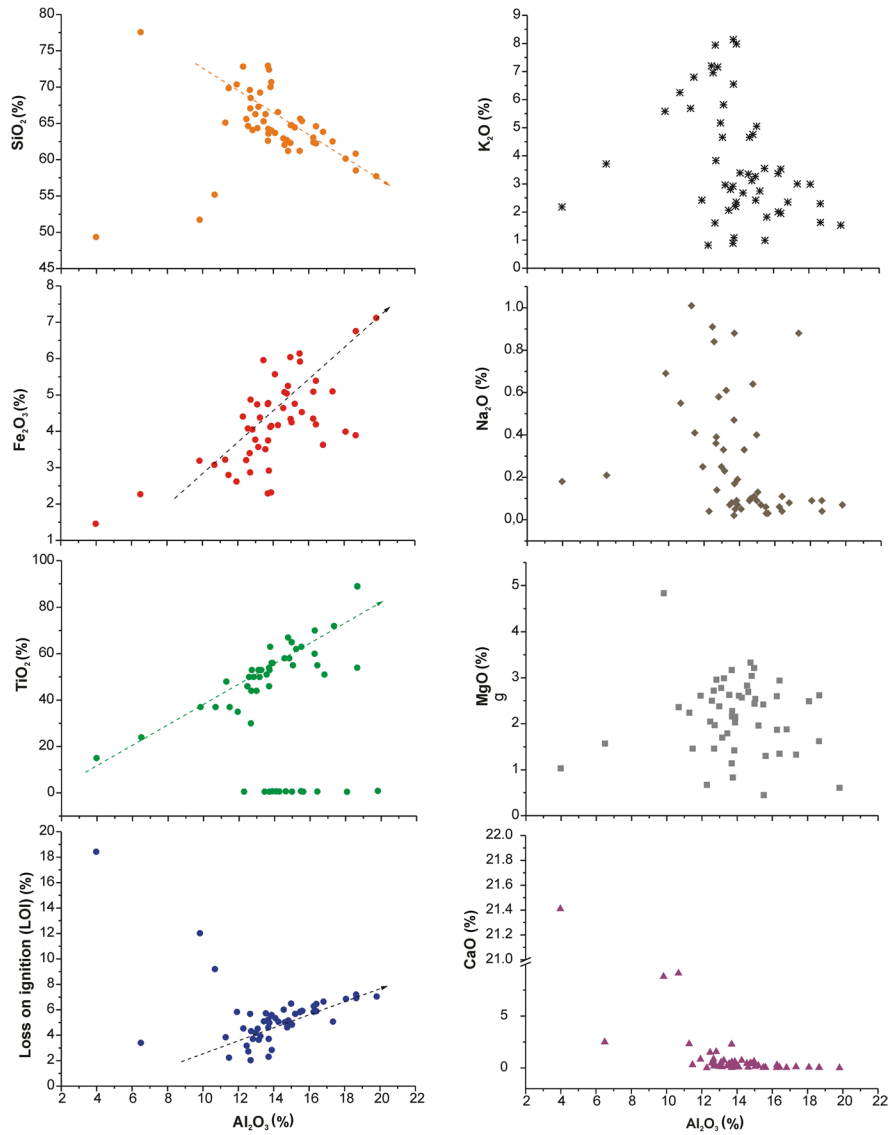

Fig. 9 Harker variation diagram, with major elements as a function of Al_2O_3

content of the facies toward the top indicates the transition from a deep-shelf marine environment, dominated by decantation and traction processes associated with low-energy tides, going toward shallower domains, with combined flows.

(3) A lateral regional variation of these facies exists throughout their exposure in the State of São Paulo, resulting from the genetic formation of the deposits and the location of their source area. This is reflected, in particular, in the facies description, as well as in terms of the mineralogy and chemical composition, where the presence of a specific mineral or element is reflected in the ceramic properties and the type of product manufactured, as well as in the economic use as a ceramic raw material.

(4) The deposits studied differed from those found in the Santa Gertrudes Ceramic Cluster, where the granulometric, chemical, and mineralogical characteristics indicate a more refractory and less flux ceramic behavior.

https://doi.org/10.1007/s42860-022-00212-6 Published online by Cambridge University Press

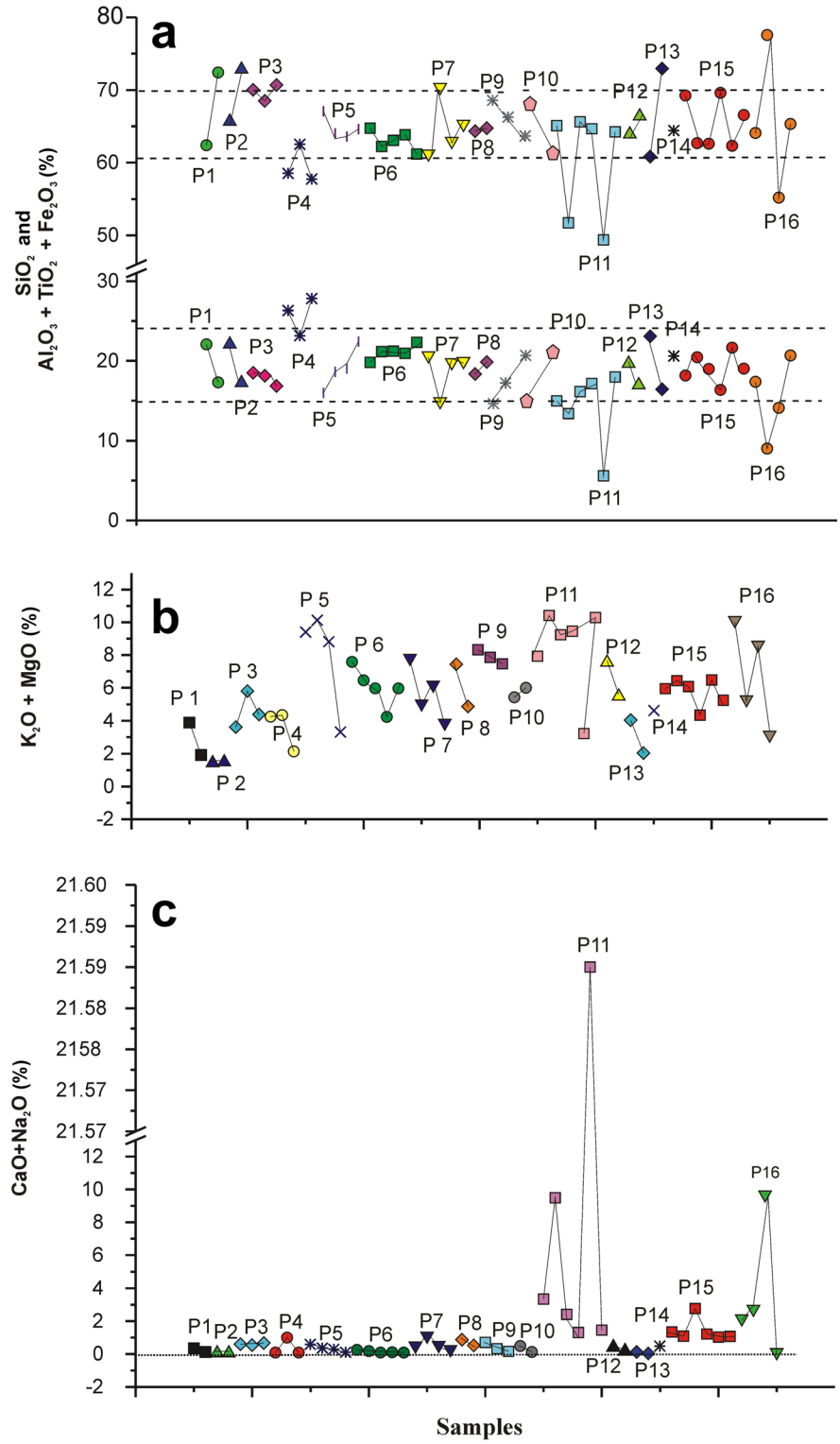

Fig. 10 Variation in concentrations of oxides in the samples of each sampled columnar profile

https://doi.org/10.1007/s42860-022-00212-6 Published online by Cambridge University Press

Table 5 Ceramic characterization. MRF = modulus of rupture flexion after firing (kgf/cm^2). WA = water absorption (%), AP = apparent porosity (%), LFS = linear firing shrinkage, Ddry = apparent drying density (g/cm^3), and GWAs = groups of water absorption

Samples	MRF	WA	AP	LFS	Ddry	GWAs
P1-A1	302.87	11.17	22.72	4.29	1.86	BIII
P1-A2	101.47	20.23	34.99	0.16	1.78	BIII
Average	202.17	15.7	28.85	2.22	1.82	
P2-A1	82.40	22.52	22.52	1.42	1.70	BIII
P2-A2	42.15	19.99	35.09	0.48	1.79	BIII
Average	62.27	21.25	28.80	0.95	1.74	
P3-A1	190.15	12.08	23.67	4.16	1.78	BIII
P3-A2	312.01	5.37	11.65	7.59	1.76	BIIa
P3-A3	236.7	10.72	21.48	6.22	1.76	BIII
Average	246.28	9.39	18.93	6.90	1.76	
P4-A1	244.4	14.7	28.41	3.97	1.77	BIII
P4-A2	200.56	11.06	23.39	3.57	1.86	BIII
P4-A3	168.95	17.94	32.90	2.54	1.81	BIII
Average	204.63	16.32	30.65	3.36	1.82	
P5-A1	120.96	13.1	25.18	1.72	1.84	BIII
P5-A2	320.02	9.84	20.00	6.18	1.73	BIIb
P5-A3	463.05	3.81	8.60	10.26	1.59	BIb
P5-A4	221.75	13.32	26.1	4.02	1.89	BIII
Average	281.44	10.01	18.23	5.54	1.76	
P6-A1	267.49	3.82	8.70	8.67	1.79	BIIb
P6-A2	307.72	7.58	16.06	6.6	1.81	BIIb
P6-A3	392.80	4.81	10.85	10.85	1.83	BIIb
P6-A4	271.09	8.95	18.62	5.24	1.86	BIIb
P6-A5	379.00	2.18	2.18	10.39	1.80	BIb
Average	323.62	5.88	11.28	8.35	1.82	
P7-A1	420.18	0.47	1.16	10	1.83	BIa
P7-A2	110.95	11.81	22.38	2.17	1.82	BIII
P7-A3	370.62	2.41	5.66	9.89	1.78	BIb
P7-A4	140.45	18.27	33.44	4.65	1.90	BIII
Average	207.34	8.24	2.19	6.03	1.83	
P11-A1	140.00	8.61	3.22	2.88	1.92	BIII
P11-A2	100.87	16.15	3.93	1.91	1.87	BIII
P11-A3	110.02	9.89	19.98	3.24	1.82	BIII
P11-A4	220.23	4.55	10.24	7.42	1.78	BIIb
P11-A5	120.00	32.42	47.19	—	1.79	BIII
P11-A6	190.56	10.46	21.13	3.17	1.85	BIII
Average	146.94	15.62	25.76	3.72	1.83	
P15-A1	340.00	2.24	5.29	6.97	1.94	BIb
P15-A2	410.60	1.34	3.28	7.82	1.97	BIb
P15-A3	320.62	2.22	5.19	7.09	1.92	BIb
P15-A4	220.14	13.26	25.2	2.85	1.79	BIII
P15-A5	490.64	1.48	3.63	8.59	1.95	BIb
P15-A6	290.90	4.05	9.35	5.46	1.97	BIIa
Average	345.48	4.10	8.66	5.64	1.94	
P16-A1	390.70	2.10	4.90	9.27	1.97	BIb

https://doi.org/10.1007/s42860-022-00212-6 Published online by Cambridge University Press

Table 5 (continued)

Samples	MRF	WA	AP	LFS	Ddry	GWAs
P16-A2	150.30	14.67	26.33	2.19	1.92	BIII
P16-A3	160.59	13.87	26.33	3.22	1.79	BIII
P16-A4	230.77	13.07	25.92	3.93	1.95	BIII
	233.00	10.92	20.87	4.65	1.90	
Total Average	245.00	9.75	18.25	5.18	1.82	BIIb

(5) The water absorption results obtained under laboratory conditions revealed that most of the samples fall into the BIII Group, referred to as 'porous' according to ABNT; their application will focus mainly on the production of tiles for internal walls, used especially in bathrooms. Exceptions were found in samples of facies of profiles P6, P7, and P15 which have a more uniform granulometric distribution, resulting in better sintering than the clays found in the region of the Santa Gertrudes Ceramic cluster. This classifies these samples into Groups BIIb and BIb, named according to their commercial nomenclature as semi-porous and stoneware; their application is mainly in the production of tiles for floors or in the composition of ceramic masses for the production of porcelain by wet grinding. Note that ceramic tests were carried out in laboratory conditions and that industrial-scale tests are needed to verify the results.

Acknowledgements The authors gratefully acknowledge the financial support of FAPESP (São Paulo Research Foundation) Process 2012/24219-9. The second author thanks CNPq for the productivity support (Process 310734/2020-7).

Declarations

Conflict of Interest The authors declare that they have no conflict of interest

References

Associação Paulista das Cerâmicas de Revestimento-ASPACER. (2021). Panorama da indústria cerâmica paulista. https://www.aspacer.com.br/estatisticas/. Accessed 7 Oct 2021

Azzi A.A., Marek Osacký, M., Uhlík, P., Mária Čaplovičová, M., Zanardo, A., & Jana Madejová, J. (2016). Characterization of clays from the Corumbataí Formation used as raw material for ceramic industry in the Santa Gertrudes district, São Paulo, Brazil. *Applied Clay Science*, 1–11.

Beltrán, V., Sánchez, E., García-Ten, J., & Ginés, F. (1996). Materias primas empleadas en la fabricación de baldosas de pasta blanca en España. *Técnica Cerámica, 241*, 114–128.

Bergaya, F., & Lagaly, G. (2006). General introduction: Clays, clay minerals, and clay science. *Developments in Clay Science, 1*, 1–18.

Boix, A., Gargallo., M., Jordan., M.M., Segura., R., & Sanfeliu., T. (1994). Mineralogy and technological properties of clays used in the ceramic floor and wall tile sector. *Técnica Cerámica, 224*, 404–413.

Brindley, G. W., & Brown, G. (1980). X-ray Diffraction procedures for clay mineral identification. In G. W. Brindley & G. Brown (Eds.), *Crystal Structures of Clay Minerals and their X-ray Identification* (pp. 305–360). Mineralogical Society.

Christofoletti, S. R., & Moreno, M. M. T. (2011). Sustentabilidade da mineração no polo cerâmico de Santa Gertrudes, São Paulo-Brasil. *Cerâmica Industrial, 16*, 35–42.

Christofoletti, S. R., Moreno, M. M. T., & Batezelli, A. (2006). Análise de fácies da Formação Corumbataí (Grupo Passa Dois, Bacia do Paraná, Neopermiano), com vista ao emprego na indústria de revestimento cerâmico. *Revista Brasileira De Geociências, 36*, 488–498.

Christofoletti, S. R., Moreno, M. M. T., & Motta, J. F. M. (2009). La Formación Corumbataí y su importancia en la industria cerámica del estado de São Paulo-Brasil. *Matéria, 14*, 705–715.

Christofoletti, S.R., Moreno, M.M.T., Del Roveri, C., & Zanardo, A. (2010). Qualidade em cerâmica: 14 anos de pesquisa em matéria prima cerâmica. Anais do 54º Congresso Brasileiro de Cerâmica, Foz do Iguaçu, PR, Brasil.

Christofoletti, S. R., Batezelli, A., & Moreno, M. M. T. (2015). Caracterização geológica, mineralógica, química e cerâmica da Formação Corumbataí nos municípios de Tambaú, Porto Ferreira e Santa Rosa do Viterbo-SP, visando aplicação e diversificação de produtos no polo cerâmico de Santa Gertrudes. *Geociências, 34*, 24–33.

Costa, M.N.S. (2006). Diagênese e alteração hidrotermal em rochas sedimentares da Formação Corumbataí, Permiano Superior, Mina Granusso, Cordeirópolis/SP. Ph.D. thesis, Universidade Estadual Paulista, Brasil, 140pp.

Del Roveri, C., Cunha, R.A., Zanardo, A., Godoy, L.H., Moreno, M.M.T., Rocha, R.R., & Maestrelli, S.C. (2016). chemical-mineralogical and microscopic characterization of clay used as raw materials in Santa Gertrudes ceramic pole. *Materials Science Forum,* 191–194.

Dondi, M., Ercolani, G., Melandri, C., Mingazzini, C., & Marsigli, M. (1999). The chemical composition of porcelain

stoneware tiles and its influence on microstructural and mechanical properties. *Interceram, 48*, 75–83.

Dondi, M. (1999). Clay materials for ceramic tiles from the Sassuolo district (northern Apennines, Italy). Geology, composition, and technological properties. *Applied Clay Science, 15*, 337–366.

Dondi, M., Raimondo, M., & Zanelli, C. (2014). Clays and bodies for ceramic tiles: Reappraisal and technological classification. *Applied Clay Science, 96*, 91–109.

Fiori, C. (1996). Raw materials for the Italian stoneware tile industry. *Industrial Ceramics, 16*, 77–83.

Ferrari, S., & Gualtieri, A. F. (2006). The use of illitic clays in the production of stoneware tile ceramics. *Applied Clay Science, 32*, 73–81.

Galos, K. (2011b). Influence of mineralogical composition of applied ball clays on properties of porcelain tiles. *Ceramic International*, *37*, 851–861.

Kadır, S., Erman, H., & Erkoyun, H. (2011). Mineralogical and geochemical characteristics and genesis of hydrothermal kaolinite deposits within Neogene Volcanites, Kütahya (Western Anatolia), Turkey. *Clays and Clay Minerals, 59*, 250–276.

Külah, T., Kadir, S., Gürel, A., Eren, M., & Önalgil, N. (2014). Mineralogy, geochemistry, and genesis of mudstones in the Upper Miocene Mustafapaşa Member of the Ürgüp Formation in the Cappadocia region, central Anatolia, Turkey. *Clays and Clay Minerals, 62*, 267–285.

Landim, P. M. B. (1970). O Grupo Passa Dois (P) na Bacia do rio Corumbataí (SP). *Boletim Divisão Geologia e Mineralogia/DNPM, São Paulo, 252*, 103.

Manju, C.S., Nair, V.N., & Lalithambika., M. (2001). Mineralogy, geochemistry, and utilization study of the Madayi kaolin deposit, north Kerala, India. *Clays and Clay Minerals*, *49*, 355–369.

Mezzalira, S. (1964). Grupo Estrada Nova. *Boletim do Instituto Geográfico e Geológico*, *São Paulo*, 41, 63–84.

Miall, A. D. (1994). *Principles of sedimentary basin analysis* (p. 490). Springer-Verlag.

Montibeller, C. C., Beltran, R. G., Zanardo, A., Ronh, R., Del Roveri, C., Rocha, R. R., & Conceição, F. T. (2020). Geochemistry of siltstones from the Permian Corumbataí Formation from the Paraná Basin (State of São Paulo, Brazil): Insights of provenance, tectonic and climatic settings. *Journal of South American Earth Sciences, 102*, 102582.

Meneghel, E.C. (2021). Caracterização geológica e tecnológica de argilas plásticas em rochas Permianas-Carboníferas da região de Tatuí e Porto Ferreira/SP. Master Dissertation, Universidade Estadual Paulista, Brasil, 111pp.

Motta, J. F. M., Christofoletti, S. R., Garcez, L. L., Florêncio, R. V. S., Boschi, A. O., Moreno, M. M. T., & Zanardo, A. (2004). Características do pólo de revestimentos cerâmicos de Santa Gertrudes–SP, com ênfase na produção de argilas. *Cerâmica Industrial, 9*, 1–6.

Motta, J. F. M., Christofoletti, S. R., Garcez, L. L., Florêncio, R. V., Boschi, A. O., Moreno, M. M. T., Del Roveri, C., & Zanardo, A. (2005). Raw materials for ceramic tiles in the Santa Gertrudes Pole, Brazil. *Interceram, 56*, 263–267.

Murray, H. H. (1999). Applied clay mineralogy today and tomorrow. *Clay Minerals, 34*, 39–49.

Orts, M. J., Campos, B., Pico, M., & Gozalbo, A. (1993). Methods of granulometric analysis: Application in the granulometry control of raw materials. *Tile Brick International, 9*, 143–150.

Penanes, P. A., Reguera-Galan, A., Huelga-Suarez, G., Rodríguez-Castrillón, J. Á., Moldovan, M., & Alonso, J. I. G. (2022). Isotopic measurements using ICP-MS: A tutorial review. *Journal of Analytical Atomic Spectrometry, 37*, 701–726.

Perinotto, J.A.J.; & Zaine, M.F. (2008). Patrimônios naturais e história geológica da região de Rio Claro-SP. *Arquivo Público e Histórico do Município de Rio Claro, 1*, 91pp.

Rollinson, H. R. (1995). *Using geochemical data: Evaluation, presentation, interpretation* (p. 353). Longman Group.

Salvador, R. B., & Simone, L. R. L. (2010). Histórico dos estudos sobre a malacofauna fóssil da Formação Corumbataí, Bacia do Paraná, Brasil. *Revista Da Biologia, 5*, 19–23.

Smoot, T. W. (1961). Clay Minerals in the ceramic industries. *Clays and Clay Minerals, 10*, 309–317.

Sousa, S.H.M. (1985). Fácies sedimentares das formações Estrada Nova e Corumbataí no Estado de São Paulo. Master dissertation, Instituto de Geociências, Universidade de São Paulo, Brasil.

Souza, P. E. C., Christofoletti, S. R., Moreno, M. M. T., & Corrêa, V. F. (2010). A Formação Corumbataí nos municípios de Tambaú e Limeira - SP: Fonte de matéria-prima para o segmento de porcelanato e semi-grés. *Cerâmica Industrial, 15*, 30–34.

Thiry, M. (1974). Technique de préparation des minéraux argileux en vue de l´analyse aux rayons X. Centre National de la Récherche Scientifique (CNRS), Centre de Sedimentologie et Géochimie de la Surface, Strasbourg, 25 pp.

Wentworth, C. K. (1922). A scale of grade and class terms for clastic sediments. *Journal Geology, 30*, 377–392.

Zalba, P. E. (1979). Clay deposits of Las Aguilas formation, barker, Buenos Aires Province, Argentina. *Clays and Clay Minerals, 27*, 433–439.

Zanardo, A., Montibeller, C. C., Navarro, G. R. B., Moreno, M. M. T., Rocha, R. R., Del Roveri, C., & Azzi, A. A. (2016). Formação Corumbataí na região de Rio Claro/SP: Petrografia e implicações genéticas. *Geociências, 35*, 322–345.

Zanelli, C., Dondi, M., Guarini, G., Raimondo, M., Domínguez, E., Iglesias, C., & Dondi, M. (2008). The geology and mineralogy of a range of kaolins from the Santa Cruz and Chubut provinces, Patagonia (Argentina). *Applied Clay Science, 40*, 124–142.

Zanelli, C., Iglesias, C., Dominguez, E., Gardini, G., Raimondo, M., Guarini, G., & Dondi, M. (2015). Mineralogical composition and particle size distribution as a key to understand the technological properties of Ukrainian ball clays. *Applied Clay Science, 108*, 102–110.

https://doi.org/10.1007/s42860-022-00212-6 Published online by Cambridge University Press